PHYSICAL REVIEW B **92**, 020408(R) (2015)

Towards graded-index magnonics: Steering spin waves in magnonic networks

C. S. Davies,[1] A. Francis,[1] A. V. Sadovnikov,[2,3] S. V. Chertopalov,[4] M. T. Bryan,[5] S. V. Grishin,[2] D. A. Allwood,[5] Y. P. Sharaevskii,[2] S. A. Nikitov,[2,3] and V. V. Kruglyak[1,*]

[1]*School of Physics, University of Exeter, Stocker Road, Exeter EX4 4QL, United Kingdom*

[2]*Laboratory "Metamaterials," Saratov State University, Saratov 410012, Russia*

[3]*Kotel'nikov Institute of Radioengineering and Electronics, Russian Academy of Sciences, Moscow 125009, Russia*

[4]*Donetsk National University, 24 Universitetskaya Street, Donetsk 83001, Ukraine*

[5]*Department of Materials Science and Engineering, University of Sheffield, Sheffield S1 3JD, United Kingdom*

(Received 2 February 2015; revised manuscript received 29 June 2015; published 20 July 2015)

Magnonics explores precessional excitations of ordered spins in magnetic materials—so-called spin waves—and their use as information and signal carriers within networks of magnonic waveguides. Here, we demonstrate that the nonuniformity of the internal magnetic field and magnetization inherent to magnetic structures creates a medium of graded refractive index for propagating magnetostatic waves and can be used to steer their propagation. The character of the nonuniformity can be tuned and potentially programmed using the applied magnetic field, which opens exciting prospects for the field of graded-index magnonics.

DOI: 10.1103/PhysRevB.92.020408 PACS number(s): 75.30.Ds, 75.50.Bb, 75.78.Cd, 75.78.Jp

Over the past decade, magnonics (the study of spin waves—precessional excitations of ordered spins in magnetic materials [1]) has emerged as one of the most rapidly growing research fields in magnetism [2,3]. Moreover, recent advances in the understanding of fundamental properties of spin waves in magnetic micro- and nanostructures have highlighted magnonics as a potential rival of or complement to semiconductor technology in the field of data communication and processing [4]. The push for miniaturization renders ferromagnetic transition metals and their alloys to be materials of choice for the fabrication of spin-wave devices [5,6]. However, loss reduction, the shortening of the wavelength of studied spin waves, and the associated miniaturization of the implemented magnonic concepts and devices remain major challenges in both experimental research and technological development in magnonics [2,3].

In this Rapid Communication, we explore an approach to meet these challenges that is based on the concept of graded-index (or gradient-index) optics [7]. As applied to spin waves, this concept is based on the following basic ideas. First, the propagation of spin waves is controlled using subwavelength, often continuously varying, magnetic nonuniformities [8,9]. This should minimize scaling of the device size with the magnonic wavelength, in contrast to, e.g., magnonic crystal based approaches [3], and thereby ease the associated patterning resolution requirements. Indeed, nonuniform effective magnetic field and magnetization configurations have been shown to confine [10,11] and channel [12–15] spin waves, to continuously modify their character [16–18], and to enable their coupling to essentially uniform free space microwaves [19,20]. Here, we go further by exploiting in addition the anisotropic dispersion inherent to spin waves dominated by the dynamic magneto-dipole field—so-called magnetostatic spin waves [1]. The symmetry axis of the anisotropic magnetostatic dispersion coincides with the direction of the magnetization [21–23]. This anisotropic dispersion leads to the formation of nondiffracting caustic spin-wave beams [24–30] and to anomalous spin-wave reflection, refraction, and diffraction [31–35]. Here, we explore these ideas in networks of magnonic waveguides [6,8,12–20,24,29,36], in which not only the internal magnetic field and the magnetization, but also the associated anisotropic dispersion are nonuniform and contribute significantly to the observed switching of the direction of spin-wave propagation. In excellent agreement with numerical micromagnetic modeling [37], our results of the time-resolved scanning Kerr microscopy (TRSKM) [19,20] imaging of magnetostatic spin waves propagating in Permalloy magnonic waveguides not only supply further evidence of feasibility, but also uncover exciting opportunities ahead of the "graded-index magnonics" theme.

In our experiments, we adopted the scheme of spin-wave excitation from Refs. [19,20] [Fig. 1(a)], which could be traced back to the Schlömann mechanism [38]. A micrometer scale H-shaped Permalloy microstructure [Fig. 1(b)] was placed onto a much wider signal line of a coplanar waveguide (CPW) connected to a microwave source. The sample was biased by a uniform in-plane static magnetic field $\boldsymbol{H}_{\mathrm{B}}$. Due to the effect of the magnetic shape anisotropy [1], different sample regions had different magnetic resonance frequencies. Tuning the microwave frequency of the virtually uniform magnetic field from the CPW to these resonances could, therefore, be used to selectively excite magnetization precession in particular sample regions. At the boundaries between resonating and nonresonating regions of the sample (i.e., the T junctions between the different straight parts of the microstructure), the resonantly excited magnetization acted as a magnonic source. Indeed, the broken translational symmetry at the T junctions effectively enabled the (otherwise forbidden) coupling of the microwave electromagnetic field to propagating spin waves of at least three orders of magnitude shorter wavelength. The frequency of the excited spin waves was equal to that of the excitation microwave field, while their wave vector was dictated by the dispersion relation of magnetostatic spin waves, as expected at the micrometer length scales in Permalloy [1,19–23]. The spin waves were imaged by TRSKM near one of the T junctions, as shown schematically in Fig. 1(b). By combining images acquired for different phases of the

*Corresponding author: v.v.kruglyak@exeter.ac.uk

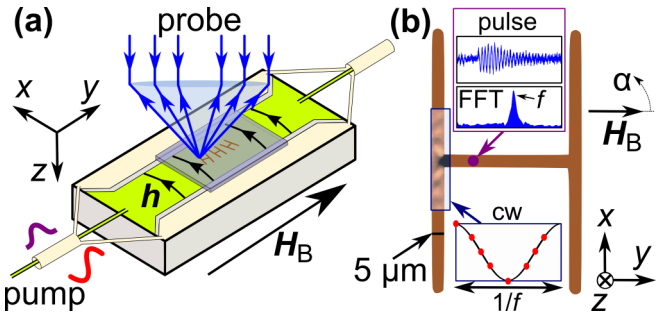

FIG. 1. (Color online) A schematic of the TRSKM experiment. (a) The Permalloy microstructures are mounted on top of the CPW, producing a microwave magnetic field $\boldsymbol{h}$. The scanned optical probe is used to measure the out-of-plane component of the magnetization via the polar Kerr effect. (b) The sample is shown, together with a representative time-resolved Kerr signal acquired in experiments with pulsed excitation and its Fourier spectrum (top inset). In experiments with cw excitation, Kerr images of the spin waves in the highlighted region were acquired at eight time delays, shown by the red points on one cycle of the continuous wave (cw) microwave pump (bottom inset). The frequency f of the microwave is equal to that of the Fourier peak from the top inset. The bias magnetic field $\boldsymbol{H}_B$ is applied at different angles α relative to the horizontal symmetry axis of the microstructure.

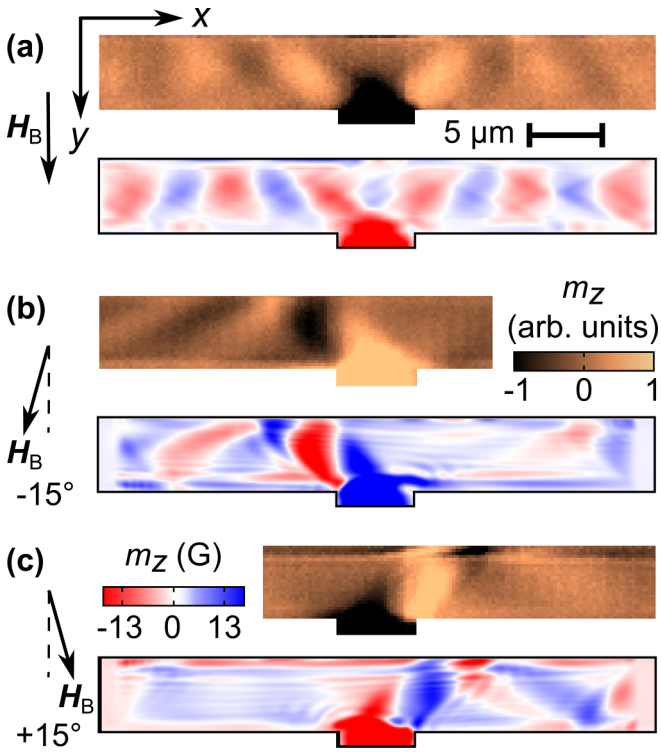

FIG. 2. (Color online) Snapshots of spin waves propagating in the arms of the Permalloy T junction. The bias magnetic field $\boldsymbol{H}_B = 500$ Oe is applied parallel (a) and at angles of $\alpha = -15^\circ$ (b) and $\alpha = +15^\circ$ (c) relative to the leg of the junction (i.e., horizontal symmetry axis from Fig. 1). In each case, the top and bottom panels show results of the TRSKM imaging and micromagnetic simulations, respectively. The frequency of the cw pump was 8.24 GHz for experiments, while for simulations it was 7.62 GHz in (a) and 7.52 GHz in (b) and (c). The difference in the frequency values is due to inevitable differences between the measured and simulated samples.

microwave excitation field [bottom inset of Fig. 1(b)], movies of the propagating spin waves were composed. Prior to the imaging experiments, the resonant frequencies of the different parts of the sample were determined by Fourier transforming the TRSKM signals acquired for a fixed position of the laser spot [top inset of Fig. 1(b)].

The characteristic TRSKM snapshots of the propagating spin waves, together with corresponding micromagnetic simulations, are presented in Fig. 2 for different orientations of the bias magnetic field of 500 Oe [39]. When the bias field is applied symmetrically, parallel to the "leg" of the T junction, the excited spin waves are observed to split equally between the two junction "arms" [Fig. 2(a)]. The phase fronts are somewhat tilted relative to the symmetry axis. When the bias magnetic field is rotated from the symmetry axis by just $\pm 15^\circ$, we observe only one spin-wave beam propagating into one of the arms [Figs. 2(b) and 2(c)]. The direction of the propagation is "switched" between the two arms by the sign of the tilt angle. In each case, the spin-wave beam propagates at an oblique angle to the arm's axis, hits its edge, and is reflected into a much broader beam, propagating approximately along the arm's length. Thereby, the sample behaves as a magnetostatic spin-wave multiplexor, i.e., as the one from Ref. [15], which is, however, controlled by a small rotation of the applied uniform rather than local magnetic field. In contrast to Ref. [15], the mechanism of spin-wave steering presented here does not require passing an electrical current underneath one of the waveguides. We also note that, apart from the local current control established in Ref. [15] and the global magnetic field control discussed here, the nonuniformity of the effective magnetic field required for the graded magnonic index functionality could be generated by a switchable microscale magnet [40] or by locally modifying the composition of the waveguide [41]. Moreover, albeit not demonstrated here, the magnetic configurations required for steering spin waves in a particular direction could be, at least in principle, created by exploiting hysteresis in suitable magnetic structures, indeed paving the way to reconfigurable magnonic waveguiding [3].

The experiments and simulations consistently reveal that the phase fronts in the incident and scattered beams are both significantly tilted relative to the direction of propagation. Together with the difference in the incidence and reflection angles, the tilt of the phase fronts suggests the effect of the highly anisotropic dispersion inherent to magnetostatic waves [1,23,31–34]. Hence, we interpret our observations in terms of the spatial distributions of the orientations of the magnetization and the value of the internal magnetic field, which determine the local axis and strength of the dispersion's anisotropy. Based on the convincing agreement between the measured and numerically simulated results, we have applied the theory from Ref. [23] to the numerically computed static magnetization and field distributions [Fig. 3(a)] so as to derive the local directions of the wave vectors and group velocities of the propagating spin waves [Fig. 3(d)], as schematically illustrated in Figs. 3(b) and 3(c).

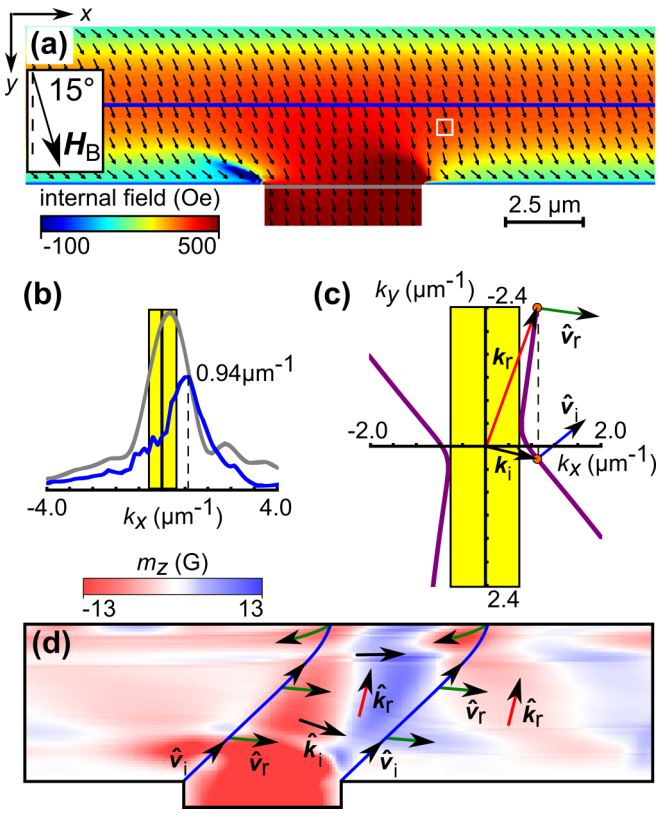

FIG. 3. (Color online) Spin waves in an asymmetrically magnetized Permalloy T junction. (a) The calculated distributions of the static magnetization (arrows) and the projection of the internal magnetic field onto the magnetization (color scale) are shown for the magnetic field of $\boldsymbol{H}_B = 500$ Oe applied at 15° to the vertical symmetry axis. Each arrow represents the average of 5 × 5 mesh cells. (b) k_x spectra of the dynamic magnetization distributions across the leg [gray line in (a)] and along the arms [blue line in (a), amplified ×5] of the T junction excited at 7.52 GHz are shown by the gray and blue curves, respectively. The k_x value of 0.94 μm^{-1}, indicated by a dashed line, corresponds to maximum spin-wave Fourier amplitude. (c) A construction illustrating the extraction of the group velocities of the incident (index "i") and reflected (index "r") beams is shown for the white boxed pixel in (a). For the specific k_x value of 0.94 μm^{-1} [which is indicated by the vertical dashed lines here and in (b)], the group velocities are perpendicular to the characteristic isofrequency curves (purple). The k_y value is given by the crossing of the dashed line and the isofrequency curve. Here and in (b), the region shaded yellow has the same size and represents the range of forbidden k_x values, as calculated for the white boxed pixel and for pixels on the gray line in (a), respectively. (d) The extracted directional unit vectors of the group velocities $\hat{\boldsymbol{v}}$ and wave vectors $\hat{\boldsymbol{k}}$ are shown for k_x values shown by the vertical dashed lines in (b) and (c).

The precessing magnetization in the leg of the T junction is confined to its width, which results in a broad spectrum of the k_x projection of the magnonic in-plane wave vector [Fig. 3(b)]. Then, for each k_x value, the isofrequency curve corresponding to the excitation frequency returns an allowed (by the magnetostatic dispersion relation) value of k_y, while the normal to the isofrequency curve shows the direction of the group velocity [Fig. 3(c)] [23–26]. The uniformity of the field and magnetization distributions in the arms along the x axis (starting from about 1 μm from the leg-arm boundary) ensures conservation of the k_x value of the spin wave propagating across the arm's width. In contrast, the values of k_y and the group velocity adjust adiabatically according to the variation of the internal field magnitude and direction of the magnetization across the arm's width. The nonuniformity also leads to a distributed partial reflection of the spin-wave amplitude. The directions of the incident and reflected waves are given by plots similar to that shown in Fig. 3(c), but constructed for local values of the internal magnetic field and directions of the magnetization, while the strengths of the reflections are given by the speed of their variation. The resulting wave field is then given by the superposition of the incident wave and the partial scattered waves.

In the specific case considered here, the magnonic wave vectors form large (often close to 90°) angles relative to the local directions of the magnetization. This corresponds to the Damon-Eshbach magnetostatic surface wave geometry [1,21,22]. The corresponding characteristic isofrequency curves are depicted in Fig. 3(c). Apart from the small region at small wave vectors, the curve consists of nearly straight lines. This leads to the virtually same direction of the magnonic group velocity for a wide range of wave vectors, giving rise to the formation of spin-wave caustic beams [24,26]. This explains our observation of the strongly directional beam emitted from the leg-arm boundary (but not the absence of the other beam). Due to the inhomogeneities of the internal field and magnetization [Fig. 3(a)], the beam curves slightly [42–45] and experiences distributed scattering, with the group velocities of the scattered waves being roughly aligned with the arm's length [Fig. 3(d)]. The distributed character of the scattering is evident from the fact that the group velocity of the reflected beam switches direction near the far edge of the arm [Fig. 3(d)], leading to the phenomenon of "back reflection" [23]. Furthermore, the reflected beam does not have the characteristic focused character inherent to caustics since its direction of propagation is dictated by the lateral confinement within the arm's width rather than by the anisotropic dispersion. As the group velocity is neither parallel nor perpendicular to the magnetization in the arm (in which case the group and phase velocities would be collinear), the phase fronts are tilted, again as dictated by the construction in Fig. 3(c). The latter effect also explains the tilted phase fronts observed in Fig. 2(a) and the asymmetry of the k_x spectrum of the magnetization distribution in the leg of the sample [Fig. 3(b)].

The magnetostatic dispersion relation forbids the excitation of Damon-Eshbach spin waves with small k_x values, as schematically illustrated in Figs. 3(b) and 3(c). This is partly (but not solely) responsible for the absence of the spin-wave propagation into the left arm of the sample, as the majority of the spectral amplitude for negative k_x values is concentrated in the "forbidden range" [Fig. 3(b)]. In addition, and quite surprisingly, we find that the beam formed from spin waves in the "allowed" range of negative k_x values cannot possibly propagate into the left arm of the junction either. Indeed, the beam is curved into the nearest edge of the left arm, from which it is then scattered backwards into the right arm [39]. This complete disappearance of one of the beams in favor of the other one is in striking contrast to the bare tilting of magnetostatic spin-wave caustic beams observed

in large patches of uniform yttrium-iron-garnet (YIG) in Ref. [26].

Our results of imaging experiments and micromagnetic simulations demonstrate the efficiency of steering magnetostatic spin waves in networks of magnonic waveguides controlled by the external magnetic field. In line with the concept of graded-index magnonics, the externally controlled nonuniformity of the magnetization and internal magnetic field distributions play the key role in defining the spatial variation of the magnonic dispersion and thereby the direction of the spin-wave propagation. However, we note that the anisotropy of the magnetostatic spin-wave dispersion is only present at micrometer to millimeter length scales, impeding miniaturization of any magnonic devices that would exploit this effect. Yet, the nonuniformity of the internal magnetic field and the magnetization persists to much shorter length scales and could still lead to useful device concepts [10–13,46]. Moreover, on the nanometer length scales, the nonuniform exchange field (completely neglected here) becomes more important and could therefore be exploited [14,47,48], while additional opportunities arise from the use of the highly localized magnetic field due to magnetic domain walls [49,50]. At the same time, the micrometer to millimeter scale (e.g., YIG-based) magnonic devices should still find application in microwave signal processing. The main challenge of graded-index magnonics is that the configurations of the internal magnetic field and the static magnetization in magnetic nano- and microstructures are not arbitrary, but are determined by the magnetostatic Maxwell equations. This limits the range of magnetic configurations that could be exploited. The search for such configurations, which could be stabilized by the sample's shape [3,8,17,20,27], application of nonuniform external magnetic field [15], or perhaps local engineering of the magnetic material properties [5], represents a broad research topic on its own.

In conclusion, we have demonstrated how the nonuniformity of the internal magnetic field and magnetization in networks of magnonic waveguides can be used to steer the propagation of magnetostatic spin waves. The character of the nonuniformity can be tuned (and potentially programmed [2,3]) using the applied magnetic field. We speculate that our findings may trigger development of technology based on the principles of graded-index magnonics.

The research leading to these results has received funding from the European Community's Seventh Framework Programme (FP7/2007-2013) under Grant Agreement No. 247556 (NoWaPhen), from the Engineering and Physical Sciences Research Council of the United Kingdom under Projects No. EP/L019876/1 and No. EP/L020696/1, from Russian Science Foundation (Project No. 14-19-00760), and the Scholarship of the President of Russian Federation (SP-313.2015.5).

[1] A. G. Gurevich and G. A. Melkov, *Magnetization Oscillations and Waves* (CRC, New York, 1996).

[2] V. V. Kruglyak, S. O. Demokritov, and D. Grundler, J. Phys. D: Appl. Phys. **43**, 264001 (2010), and references therein.

[3] M. Krawczyk and D. Grundler, J. Phys.: Condens. Matter **26**, 123202 (2014), and references therein.

[4] International Technology Roadmap for Semiconductors (ITRS) 2013 edition: Emerging Research Devices, http://www.itrs.net/Links/2013ITRS/Summary2013.htm (accessed 9 May 2014).

[5] S. Trudel, O. Gaier, J. Hamrle, and B. Hillebrands, J. Phys. D: Appl. Phys. **43**, 193001 (2010), and references therein.

[6] T. Schwarze and D. Grundler, Appl. Phys. Lett. **102**, 222412 (2013).

[7] E. W. Marchand, *Gradient Index Optics* (Academic Press, London, 1978).

[8] Y. Au, M. Dvornik, O. Dmytriiev, and V. V. Kruglyak, Appl. Phys. Lett. **100**, 172408 (2012).

[9] R. Huber, T. Schwarze, and D. Grundler, Phys. Rev. B **88**, 100405 (2013).

[10] J. Jorzick, S. O. Demokritov, B. Hillebrands, M. Bailleul, C. Fermon, K. Y. Guslienko, A. N. Slavin, D. V. Berkov, and N. L. Gorn, Phys. Rev. Lett. **88**, 047204 (2002).

[11] C. Bayer, J. P. Park, H. Wang, M. Yan, C. E. Campbell, and P. A. Crowell, Phys. Rev. B **69**, 134401 (2004).

[12] V. E. Demidov, S. O. Demokritov, K. Rott, P. Krzysteczko, and G. Reiss, Appl. Phys. Lett. **92**, 232503 (2008).

[13] G. Duerr, K. Thurner, J. Topp, R. Huber, and D. Grundler, Phys. Rev. Lett. **108**, 227202 (2012).

[14] X. Xing, Y. Yu, S. Li, and X. Huang, Sci. Rep. **3**, 2958 (2013).

[15] K. Vogt, F. Y. Fradin, J. E. Pearson, T. Sebastian, S. D. Bader, B. Hillebrands, A. Hoffmann, and H. Schultheiss, Nat. Commun. **5**, 3727 (2014).

[16] V. E. Demidov, J. Jersch, S. O. Demokritov, K. Rott, P. Krzysteczko, and G. Reiss, Phys. Rev. B **79**, 054417 (2009).

[17] V. E. Demidov, M. P. Kostylev, K. Rott, J. Münchenberger, G. Reiss, and S. O. Demokritov, Appl. Phys. Lett. **99**, 082507 (2011).

[18] H. G. Bauer, J.-Y. Chauleau, G. Woltersdorf, and C. H. Back, Appl. Phys. Lett. **104**, 102404 (2014).

[19] Y. Au, T. Davison, E. Ahmed, P. S. Keatley, R. J. Hicken, and V. V. Kruglyak, Appl. Phys. Lett. **98**, 122506 (2011).

[20] M. Arikan, Y. Au, G. Vasile, S. Ingvarsson, and V. V. Kruglyak, J. Phys. D: Appl. Phys. **46**, 135003 (2013).

[21] R. W. Damon and J. R. Eshbach, J. Phys. Chem. Solids **19**, 308 (1961).

[22] B. A. Kalinikos and A. N. Slavin, J. Phys. C **19**, 7013 (1986).

[23] A. V. Vashkovsky and E. H. Lock, Phys. Usp. **49**, 389 (2006).

[24] V. Veerakumar and R. E. Camley, Phys. Rev. B **74**, 214401 (2006).

[25] V. E. Demidov, S. O. Demokritov, D. Birt, B. O'Gorman, M. Tsoi, and X. Li, Phys. Rev. B **80**, 014429 (2009).

[26] T. Schneider, A. A. Serga, A. V. Chumak, C. W. Sandweg, S. Trudel, S. Wolff, M. P. Kostylev, V. S. Tiberkevich, A. N. Slavin, and B. Hillebrands, Phys. Rev. Lett. **104**, 197203 (2010).

[27] S. Mansfeld, J. Topp, K. Martens, J. N. Toedt, W. Hansen, D. Heitmann, and S. Mendach, Phys. Rev. Lett. **108**, 047204 (2012).

[28] Y. Au, M. Dvornik, T. Davison, E. Ahmad, P. S. Keatley, A. Vansteenkiste, B. Van Waeyenberge, and V. V. Kruglyak, Phys. Rev. Lett. **110**, 097201 (2013).

[29] T. Sebastian, T. Brächer, P. Pirro, A. A. Serga, B. Hillebrands, T. Kubota, H. Naganuma, M. Oogane, and Y. Ando, Phys. Rev. Lett. **110**, 067201 (2013).

[30] R. Gieniusz, H. Ulrichs, V. D. Bessonov, U. Guzowska, A. I. Stognii, and A. Maziewski, Appl. Phys. Lett. **102**, 102409 (2013).

[31] A. V. Vashkovskii, A. V. Stalmakhov, and D. G. Shakhnazaryan, Izv. Vyssh. Uchebn. Zaved., Fiz. **31**, 67 (1988).

[32] A. V. Vashkovskii and V. I. Zubkov, J. Commun. Technol. Electron. **48**, 131 (2003).

[33] A. V. Vashkovskii and E. G. Lokk, Phys. Usp. **47**, 601 (2004).

[34] E. H. Lock, Phys. Usp. **51**, 375 (2008).

[35] R. Gieniusz, V. D. Bessonov, U. Guzowska, A. I. Stognii, and A. Maziewski, Appl. Phys. Lett. **104**, 082412 (2014).

[36] T. Brächer, P. Pirro, J. Westermann, T. Sebastian, B. Lagel, B. Van de Wiele, A. Vansteenkiste, and B. Hillebrands, Appl. Phys. Lett. **102**, 132411 (2013).

[37] M. Dvornik, Y. Au, and V. V. Kruglyak, Top. Appl. Phys. **125**, 101 (2013).

[38] E. Schlömann, J. Appl. Phys. **35**, 159 (1964).

[39] See Supplemental Material at http://link.aps.org/supplemental/10.1103/PhysRevB.92.020408 for additional details of the TRSKM measurements and micromagnetic simulations, and movies of the spin-wave propagation associated with the presented images.

[40] L. O'Brien, D. Petit, E. R. Lewis, R. P. Cowburn, D. E. Read, J. Sampaio, H. T. Zeng, and A.-V. Jausovec, Phys. Rev. Lett. **106**, 087204 (2011).

[41] S. Urazhdin, V. E. Demidov, H. Ulrichs, T. Kendziorczyk, T. Kuhn, J. Leuthold, G. Wilde, and S. O. Demokritov, Nat. Nanotechnol. **9**, 509 (2014).

[42] This is a spin-wave analog of the mirage effect, well known in transformation optics and photonics [43,44] and recently also demonstrated theoretically in magnonics [45]. The discussion of the effect is, however, beyond the scope of this Rapid Communication.

[43] J. B. Pendry, D. Schurig, and D. R. Smith, Science **312**, 1780 (2006).

[44] U. Leonhardt, Science **312**, 1777 (2006).

[45] P. Gruszecki, J. Romero-Vivas, Yu. S. Dadoenkova, N. N. Dadoenkova, I. L. Lyubchanskii, and M. Krawczyk, Appl. Phys. Lett. **105**, 242406 (2014).

[46] X. J. Xing, S. W. Li, X. H. Huang, and Z. G. Wang, AIP Adv. **3**, 032144 (2013).

[47] V. S. Tkachenko, A. N. Kuchko, M. Dvornik, and V. V. Kruglyak, Appl. Phys. Lett. **101**, 152402 (2012).

[48] V. S. Tkachenko, A. N. Kuchko, and V. V. Kruglyak, Low Temp. Phys. **39**, 163 (2013).

[49] R. Hertel, W. Wulfhekel, and J. Kirschner, Phys. Rev. Lett. **93**, 257202 (2004).

[50] G. Duerr, R. Huber, and D. Grundler, J. Phys.: Condens. Matter **24**, 024218 (2012), and references therein.